Journal of Alloys and Compounds 513 (2012) 420–424

Contents lists available at SciVerse ScienceDirect

Journal of Alloys and Compounds

journal homepage: www.elsevier.com/locate/jallcom

Synthesis and electromagnetic characteristics of $BaFe_{12}O_{19}$/ZnO composite material

Wei Chen, Ji Zheng*, Yan Li

Department of Materials Science and Engineering, Tianjin University, Tianjin 300072, People's Republic of China

ARTICLE INFO

Article history:
Received 24 September 2011
Received in revised form 16 October 2011
Accepted 18 October 2011
Available online 25 October 2011

Keywords:
Hexaferrites
ZnO
Microwave absorption
Complex permeability
Complex permittivity

ABSTRACT

$BaFe_{12}O_{19}$/ZnO composites were fabricated in large scale via a simple solution method. The phase structures, morphologies, particle size, chemical compositions of the composites have been characterized by X-ray diffraction (XRD), field emission scanning electron microscope (FESEM). The test of microwave absorption was carried out by using the network analyzer Agilent HP-8722ES. The maximum microwave loss reaches 37.5 dB and bandwidth with the loss above 10 dB is about 4 GHz in the 13.7–18.0 GHz range which indicate that $BaFe_{12}O_{19}$/ZnO composites have potential applications as electromagnetic wave absorber.

1. Introduction

Electromagnetic (EM) wave absorbing materials have attracted increasing attention due to the expanded electromagnetic interference (EMI) problems arising from the expanding use of communication devices, such as mobile telephones, local area network systems, and radar systems. An extensive amount of researches has been devoted to exploiting a type of microwave-absorption materials with properties of a wide frequency range, a strong absorption, a low density and a high resistivity in the GHz range [1–9]. The conventional absorbing materials such as ferrites and metallic materials have been studied widely [1–6].

Ferrites serve as better EM-wave absorbers compared to their dielectric counterparts on account of their excellent magnetic properties [7]. The ferrites have been the subject of continuous interest as well as the focus of many research studies in the last few decades to be utilized as microwave absorbers in the gigahertz (GHz) range due to its high saturation magnetization, large anisotropy field, excellent chemical stability and good microwave absorption properties [8,9].

It is well known that the microwave-absorption properties are determined by the relative permeability ($\mu_\gamma = \mu' - j\mu''$), the permittivity ($\varepsilon_\gamma = \varepsilon' - j\varepsilon''$), the EM impedance match, and the microstructure of the absorber [2]. The complex permeability and permittivity of ferrite materials can be easily changed by doping or compositing with other materials, which are important in determining their high frequency absorption characteristics.

On the other hand, the ZnO-based nanocomposites, such as ZnO/SiO_2 [10], Fe/ZnO [2], Ni/ZnO [11], ZnO/$CoFe_2O_4$ [12], and ZnO nanotrees [13], have recently aroused an increasing attention because of their good EM-wave absorption, ease of synthesis, high-temperature steady, and lower cost.

In this paper, we have synthesized $BaFe_{12}O_{19}$ powder by sol–gel auto-combustion method and co-precipitation way. Zinc oxide was composited with barium ferrite by forced hydrolysis of zinc acetate at surface of $BaFe_{12}O_{19}$ particles in Diethylene Glycol (DEG). The crystalline structure, microstructure, microwave absorption properties and the effect of ZnO on the surface of $BaFe_{12}O_{19}$ are discussed. Our goal is to gain insight into the correlations between the microstructure and the physical properties of the hybrid particles in order to further experiment its characteristics for different applications.

2. Experimental

2.1. Preparation of barium ferrite powder

The starting materials of sol–gel auto-combustion method were iron nitrate, barium nitrate, citric acid and ammonia, all of analytic purity. Appropriate amounts of $Fe(NO_3)_3 \cdot 9H_2O$ and $Ba(NO_3)_2$, in a Fe/Ba molar ratio of 11, were dissolved in a minimum amount of deionized water. Citric acid was then added to the prepared aqueous solution to chelate Ba^{2+} and Fe^{3+} in the solution. The molar ratio of citric acid to total moles of nitrate ions was adjusted at 1:1. An ammonia solution was added to adjust the pH value to 7.0. The solution was slowly evaporated at 80 °C until a viscous gel formed. The dry gel obtained after dried in 110 °C was ignited

* Corresponding author. Tel.: +86 15202266283; fax: +86 02227404724.
E-mail addresses: chw015@126.com, zheng.ji@tju.edu.cn, chw015@gmail.com (J. Zheng).

0925-8388/$ – see front matter © 2011 Elsevier B.V. All rights reserved.
doi:10.1016/j.jallcom.2011.10.060

in air and burnt out to form a brown-colored loose powder. Finally, this precursor powders were calcined at 900 °C for 2 h.

2.2. Preparation of composite

The as-prepared $BaFe_{12}O_{19}$ powder was milled in a QM-BP Planetary ball milling machine (Nanjing NanDa instrument Plant, China) at room temperature for 10 h. The ball-to-powder weight ratio was 10:1. The milling was conducted using agate balls with diameters between 5 and 13 mm. A little alcohol was added into the dispersing liquid in order to avoid reaction between the powder and balls, and the adherence of powders to canister. The milling speed was 520 rpm. The ball milled $BaFe_{12}O_{19}$ powder was then dispersing in 40 ml Diethylene Glycol forming $BaFe_{12}O_{19}$ colloidal solution.

$Zn(Ac)_2$ in Diethylene Glycol (DEG) dispersion was obtained by dispersing $Zn(Ac)_2$ (3 g, 16.3 mmol) in 80 mL DEG in the presence of PVP (2 mL, 4.17 mmol). The solution was then mixed with $BaFe_{12}O_{19}$ colloidal solution in a 250 mL three-neck round-bottom flask coupled with a condenser. After being degassed and purged with argon 3 times, the mixture was slowly heated to 200 °C and kept at this temperature for 60 min. The heat source was then removed and the solution was allowed to cool to room temperature. Subsequently the black $BaFe_{12}O_{19}$/ZnO precipitate was separated by magnet from the product mixture and washed by ethanol several times. The black precipitate was dried at 60 °C and then heated to 400 °C and kept at this temperature for 1 h resulting $BaFe_{12}O_{19}$/ZnO powder.

2.3. Measurements

The crystalline structure of the composite was investigated with X-ray diffraction (XRD). The XRD spectra of the powders were made to use Cu Kα radiation and the diffraction points were recorded from 20° to 80°. Scanning electron microscopy (SEM) examinations were performed employing a Hatchi S-4800, equipped with an energy dispersive spectrometer (EDX). The specimen for measurement of EM parameters was prepared by uniformly mixing 80 wt% $BaFe_{12}O_{19}$/ZnO powder with paraffin and made into a toroidal shape (φ_{out}: 7.00 mm and φ_{in}: 3.04 mm), with a height of 2.00 mm. The relative permittivity and permeability values of the specimen were measured between 2 and 18 GHz using a network analyzer Agilent HP-8722ES.

3. Results and discussion

3.1. Crystalline structure analysis

Fig. 1 shows the XRD patterns of the pure barium ferrite, $BaFe_{12}O_{19}$/ZnO composite sample and ZnO. The diffraction peaks shown in Fig. 1(a) can be well indexed to the hexagonal crystal-structured barium ferrite (JCPDS file No. 39-1433). Fig. 1(b) shows XRD pattern of the barium ferrite–zinc oxides composite. Compared with Fig. 1(a), most diffraction peaks of the pattern show well agreement with the pure barium ferrite XRD pattern. The XRD pattern of zinc oxides is also given for comparison. It was observed that peaks indicated by▼ in Fig. 1(a) match well with the pattern of ZnO, which shows the existence of ZnO and indicates that $BaFe_{12}O_{19}$/ZnO heterostructure were formed during the ZnO synthesize process.

3.2. Morphology

FE-SEM images of the as-prepared powders are shown in Fig. 2. It can be seen from Fig. 2(a) and (b) that particle shape of $BaFe_{12}O_{19}$ sample prepared by sol–gel auto-combustion method is mainly granular and that the surface of particles is relative smooth. The particle size is below 3 μm and the distribution of particle size is of disparity. Fig. 2(c) and (d) shows microstructure and morphology of $BaFe_{12}O_{19}$/ZnO composite. Most of the particles show spherical shape and the average particle size is about 0.5 μm. It can be seen that the barium ferrite powder is successfully coated with nanosized zinc oxides. The surface of the as-synthesized powders was constructed by heterogeneous nucleation of ZnO at the surface of barium ferrite particles and looks very rough and granulated. Although the synthesis process was carried out at relative low temperature (200 °C) and with the aid of ultrasonic wave dispersion, further study is also needed to disperse the powder better.

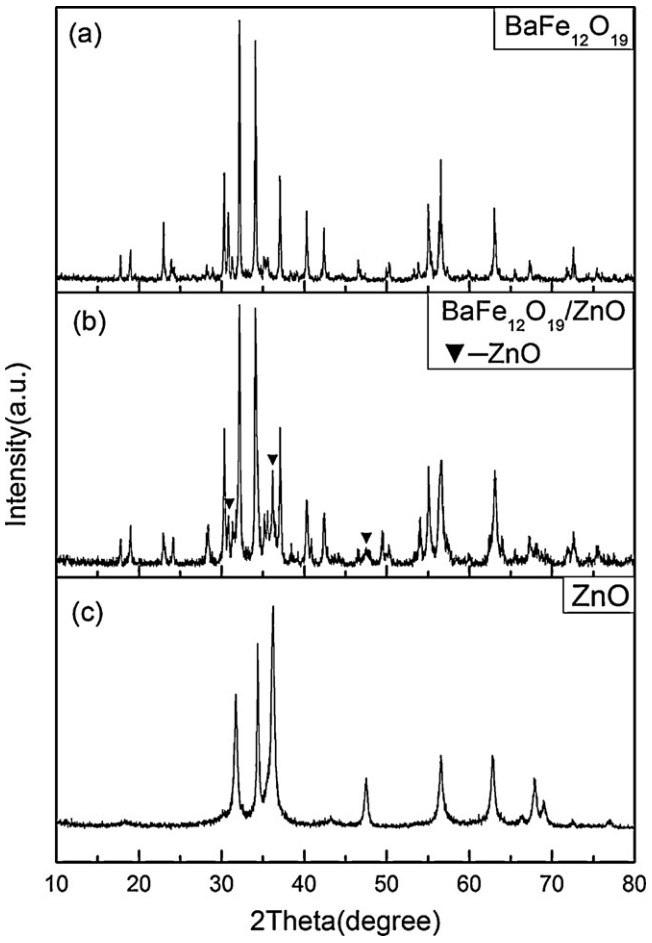

Fig. 1. XRD patterns of the as-prepared $BaFe_{12}O_{19}$ (a), $BaFe_{12}O_{19}$/ZnO composite (b) and ZnO (c).

3.3. The complex permittivity and permeability spectra

The frequency dependency on the real part (ε') and the imaginary part (ε'') of the complex permittivity in the range of 2–18 GHz for the as-prepared samples are shown in Fig. 3. The two samples exhibit a similar variety trend of the real part and the imaginary part of complex permittivity (ε', ε'') as a function of frequency. The real permittivity ε' fluctuates slightly in the whole frequency range, while the imaginary permittivity ε'' shows an increase trend in the whole frequency range. As can be seen in Fig. 3, there are frequency-intervals in which the permittivity presents resonant characteristics. The local maxima can be found before/after the resonant frequencies on the permittivity curve; three peaks can also be observed near the resonant frequencies on the ε'' curve. These phenomena are the typical characteristics of nonlinear resonant behaviors [11]. As shown in Fig. 3, the ε' value of pure barium ferrite sample is larger than that of $BaFe_{12}O_{19}$/ZnO composite, which can be attributed to the differences on polarization and surface composition of the two samples. The polarization in ferrites has largely been attributed to the presence of Fe^{2+} ions which give rise to heterogeneous spinel structure to some extent. Since Fe^{2+} ions are easily polarizable, the larger the number of Fe^{2+} ions the higher would be the dielectric constant [14]. The pure $BaFe_{12}O_{19}$ sample is likely to have more Fe^{2+} than the $BaFe_{12}O_{19}$/ZnO composites sample due to the ZnO shell on the surfaces of $BaFe_{12}O_{19}$/ZnO particles, therefore, the dielectric constant of $BaFe_{12}O_{19}$/ZnO composites sample is lower. In Fig. 3, the imaginary permittivity of composite is larger than pure barium ferrite in the range of 11–18 GHz,

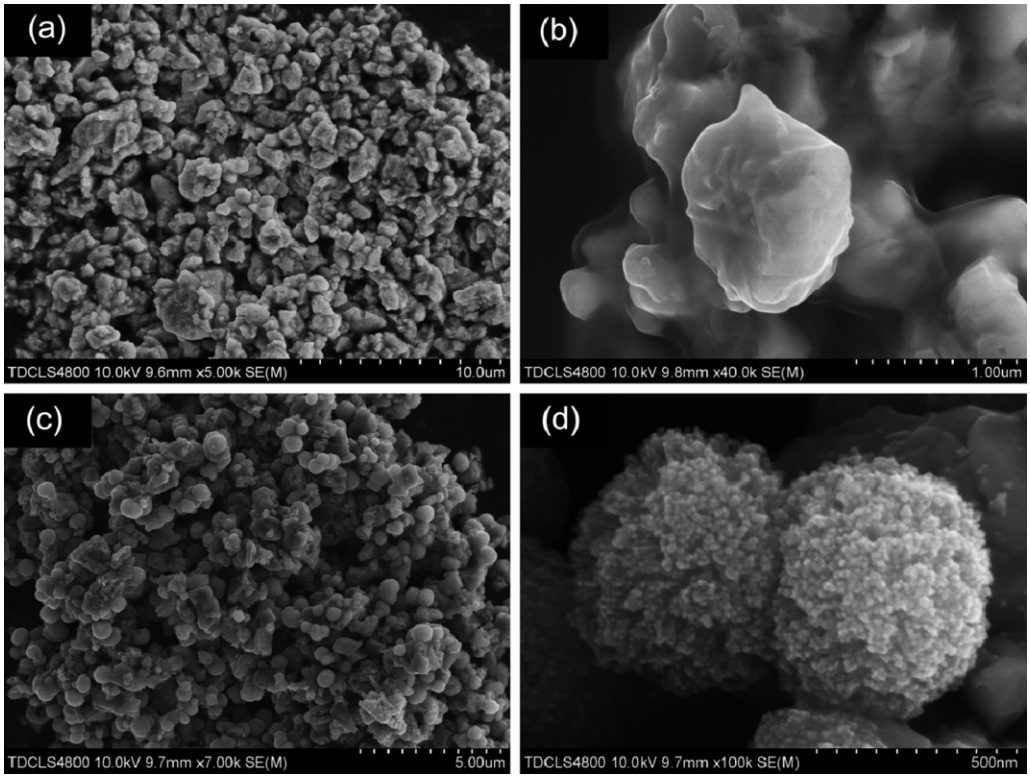

Fig. 2. FE-SEM images for $BaFe_{12}O_{19}$ particles and $BaFe_{12}O_{19}$/ZnO composite.

which suggests that the dielectric loss of $BaFe_{12}O_{19}$/ZnO composite is higher than pure $BaFe_{12}O_{19}$ in the high frequency range. In addition, the fluctuations of the real and imaginary permittivity in the range of 2–18 GHz is ascribed to displacement current lag at the heterogeneous interface, since the interfacial polarization process at the interfaces between the core and the shell, and the associated relaxation process give rise to a loss mechanism in Ba-ferrite/ZnO heterogeneous system [2].

Fig. 4 shows the real (μ') and the imaginary part (μ'') values of relative complex permeability for different samples as a function of frequency in the 2–18 GHz range. It reveals that the values of μ' and μ'' of the two samples exhibit similar variation and slight resonance absorption characters in the 2–13 GHz range, and the μ'' values of $BaFe_{12}O_{19}$/ZnO composite present a distinguishable resonance absorption peak in 13–18 GHz frequency range. In general, for polycrystalline ferrites in an AC field, resonance absorption peaks are mainly caused by two different resonance mechanisms [15]: the resonance absorption peak at high frequency is attributed to natural resonance, while the peak at low frequency is attributed to domain wall resonance. It can be found in Fig. 4 that the Ba-ferrite/ZnO show different behaviors in the variation of relative complex permeability from that of pure Ba-ferrite. As shown in Fig. 4(a), the values of μ' experience two weak peaks first after 13 GHz and then take a sudden dive between the frequency-range of 15–17 GHz. In Fig. 4(b), the imaginary permeability of

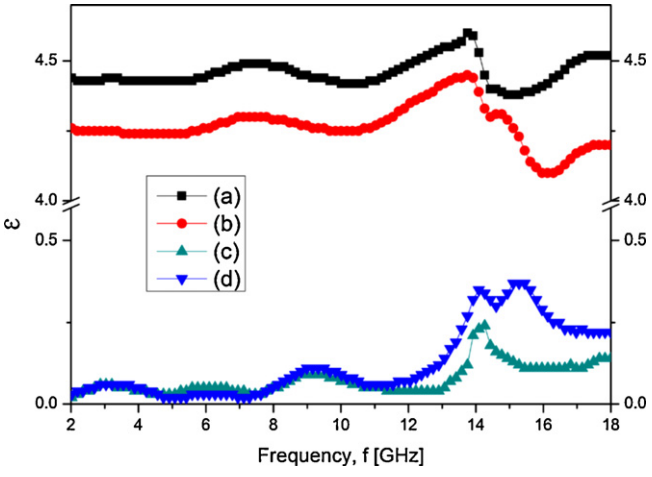

Fig. 3. Frequency dependence of real (ε') and imaginary (ε'') parts of relative complex permittivity for the powders prepared: (a) ε' of $BaFe_{12}O_{19}$, (b) ε' of $BaFe_{12}O_{19}$/ZnO composite, (c) ε'' of $BaFe_{12}O_{19}$, (d) $\varepsilon''$of $BaFe_{12}O_{19}$/ZnO composite.

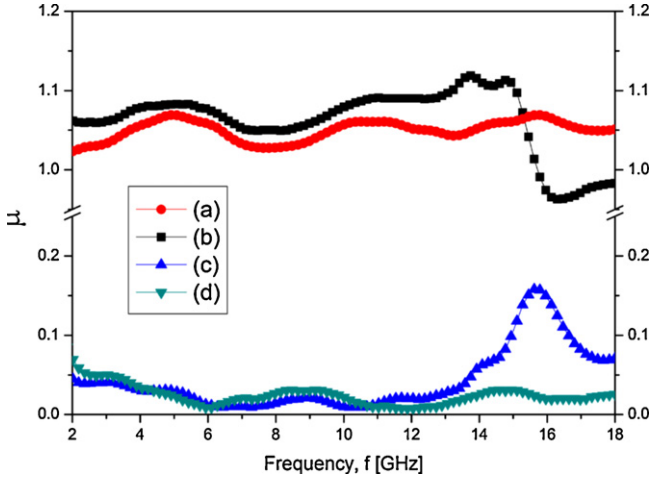

Fig. 4. Frequency dependence of real (μ') and imaginary (μ'') parts of relative complex permeability for the powders prepared: (a) μ' of $BaFe_{12}O_{19}$, (b) μ' of $BaFe_{12}O_{19}$/ZnO composite, (c) μ'' of $BaFe_{12}O_{19}$ and (d) μ'' of $BaFe_{12}O_{19}$/ZnO composite.

$BaFe_{12}O_{19}$/ZnO exhibits a distinct peak at high frequency ranging from 13 to 18 GHz. Compared with that of pure barium ferrite, the higher natural resonance frequency of $BaFe_{12}O_{19}$/ZnO composite is attributed to a larger surface anisotropic field, which is mainly affected by the shell of ZnO nanoparticles attached to the $BaFe_{12}O_{19}$ particles. Due to the smaller size of ZnO, the surface anisotropic field in the $BaFe_{12}O_{19}$/ZnO composite is larger than that in the pure barium ferrite, which leads to higher natural resonance frequency. The surface anisotropy in $BaFe_{12}O_{19}$/ZnO composite originates from broken symmetry and surface composition and becomes the main contributor to the effective anisotropy. Hence, the enhancement of the surface anisotropies in nanosized ZnO particles provides the essential contributions to the natural resonance frequency. The effects of ferrite/ZnO combination on the real and imaginary parts of permeability for the absorbing composites are demonstrated. It is this resonance that gives the corresponding reflection loss at matching frequencies according to the theory of the absorbing wall [16].

3.4. The reflection loss

According to the transmission-line theory, the reflection loss (RL) of electromagnetic waves was calculated from the relative permeability and permittivity at the given frequency and absorber thickness using the following equations [2,17]:

$$Z_{in} = Z_0 \left(\frac{\mu_r}{\varepsilon_r}\right)^{1/2} \tanh\left[j\left(\frac{2\pi fd}{c}\right)\left(\frac{\mu_r}{\varepsilon_r}\right)^{1/2}\right] \quad (1)$$

$$RL = 20\ \log\left|\frac{Z_{in} - Z_0}{Z_{in} + Z_0}\right| \quad (2)$$

where f is the frequency of the electromagnetic wave, d is the thickness of an absorber, c is the velocity of light, Z_0 is the impedance of free space, and Z_{in} is the input impedance of absorber.

According to Eqs. (1) and (2), the simulations of the reflection loss of the two composites with a thickness of 6.8 mm are shown in Fig. 5a. The $BaFe_{12}O_{19}$/ZnO–paraffin composite possesses a strong microwave absorption property. However, the $BaFe_{12}O_{19}$–paraffin composite only gives weak absorption. Fig. 5b shows simulations of reflection loss of $BaFe_{12}O_{19}$/ZnO–paraffin composite with different thicknesses in the 8–18 GHz range. The result has reflected that an optimal RL of −37.5 dB is reached at 16.1 GHz for a layer of 6.80 mm thickness, while the absorption exceeding −10 dB is obtained in the 13.7–18.0 GHz range for an absorber thickness of 6.2–9.9 mm.

It is interesting that there is only one reflection loss peak of the composite in the whole frequency range and the corresponding frequency of optimal RL is higher than that of the other barium (strontium) ferrite composites reported in several literature, i.e., $SrFe_{12}O_{19}/ZnFe_2O_4$ composite (8.7 GHz) [19], La-substituted strontium ferrite (9 GHz) [8], Ba-ferrite/PVDF composites (12.4 GHz) [20], ferrite–PU composites (12 GHz) [21], although the value of permittivity of $BaFe_{12}O_{19}$/ZnO composite is relatively lower. According to the analysis above, it has been determined that the electromagnetic absorption of the paraffin–$BaFe_{12}O_{19}$/ZnO sample is mainly ascribed to the combination of dielectric loss, which is associated with intrinsically dielectric properties and structures of the sample, as well as the magnetic loss, which is attributed to nature resonance and strong interface coupling interaction between $BaFe_{12}O_{19}$ and ZnO. In addition, the crystal defects can be introduced into barium ferrite and the dispersity of $BaFe_{12}O_{19}$ can be improved through the fast, strong and repeating impact, high-energy ball milling process, which also can be contributors of electromagnetic reflection loss in $BaFe_{12}O_{19}$/ZnO composite.

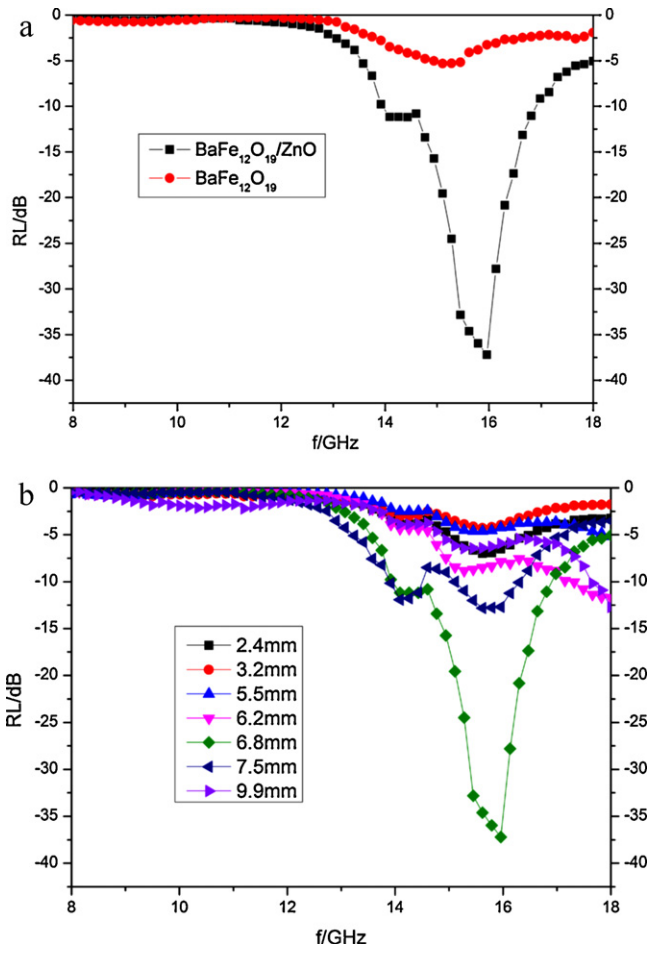

Fig. 5. Frequency dependences of reflection loss (RL) for the three samples: A, B, and C.

4. Conclusions

In summary, M-type hexagonal barium ferrite powder was prepared by self-propagating high-temperature synthesis method and co-precipitation method, respectively. $BaFe_{12}O_{19}$/ZnO composite are successfully synthesized by high-energy ball milling and subsequently forced hydrolysis of zinc acetate at surface of $BaFe_{12}O_{19}$ particles in DEG. The average particles size of composite is 0.5 μm. The maximum microwave loss reaches 37.5 dB and bandwidth with the loss above 10 dB is about 4 GHz in the 13.7–18.0 GHz range. The calculated results indicate that $BaFe_{12}O_{19}$/ZnO composite have the potentials to be utilized for fabricating electromagnetic wave absorbers.

References

[1] X.F. Zhang, X.L. Dong, H. Huang, B. Lv, J.P. Lei, C.J. Choi, J. Phys. D: Appl. Phys. 40 (2007) 5383–5387.
[2] X.G. Liu, D.Y. Geng, H. Meng, P.J. Shang, Z.D. Zhang, Appl. Phys. Lett. 92 (2008) 173117.
[3] X. Tang, B.Y. Zhao, Q. Tian, K.A. Hu, J. Phys. Chem. Solids 67 (2006) 2442–2447.
[4] A. Ohlan, K. Singh, N. Gandhi, A. Chandra, S.K. Dhawan, Appl. Phys. Lett. 93 (2008) 053114.
[5] Z. Han, D. Li, X.G. Liu, D.Y. Geng, J. Li, Z.D. Zhang, J. Phys. D: Appl. Phys. 42 (2009) 055008.
[6] A. Ghasemi, V. Sepelák, X.X. Liu, A. Morisako, IEEE Trans. Magn. Mag. 45 (2009) 2456–2459.
[7] H. Bayrakdar, J. Magn. Magn. Mater. 323 (2011) 1882–1885.
[8] N. Chen, K. Yang, M.Y. Gu, J. Alloys Compd. 490 (2010) 609–612.
[9] F. Tabatabaie, M.H. Fathi, A. Saatchi, A. Ghasemi, J. Alloys Compd. 470 (2009) 332–335.

[10] M.S. Cao, X.L. Shi, X.Y. Fang, H.B. Jin, Z.L. Hou, W. Zhou, Appl. Phys. Lett. 91 (2007) 203110.
[11] X.G. Liu, J.J. Jiang, D.Y. Geng, B.Q. Li, Z. Han, W. Liu, Z.D. Zhang, Appl. Phys. Lett. 94 (2009) 053119.
[12] J. Cao, W.Y. Fu, H.B. Yang, Q.J. Yu, Y.Y. Zhang, et al., J. Phys. Chem. B 113 (2009) 4642–4647.
[13] R.F. Zhuo, L. Qiao, H.T. Feng, J.T. Chen, D. Yan, Z.G. Wu, P.X. Yan, J. Appl. Phys. 104 (2008) 094101.
[14] B.S. Randhawa, J. Singh, Micro Nano Lett. 6 (6) (2011) 358–362.
[15] Y.P. Wu, Z.W. Li, L.F. Chen, S.J. Wang, C.K. Ong, J. Appl. Phys. 95 (2004) 4235–4239.
[16] C.-H. Penga, H.-W. Wangb, S.-W. Kanb, M.-Z. Shenb, Y.-M. Wei, S.-Y. Chen, J. Magn. Magn. Mater. 284 (2004) 113–119.
[17] J.R. Liu, M. Itoh, K.-i. Machida, Chem. Lett. 32 (2003) 394–395.
[19] N. Chen, G. Mu, X. Pan, K. Gan, M. Gu, Mater. Sci. Eng. B 139 (2007) 256–260.
[20] B.W. Li, Y. Shen, Z.X. Yue, C.W. Nan, J. Magn. Magn. Mater. 313 (2007) 322–328.
[21] S.M. Abbas, A.K. Dixit, R. Chatterjee, T.C. Goel, J. Magn. Magn. Mater. 309 (2007) 20–24.